Mixing Models as Integer Factorization: A Key to Sample Preparation with Microfluidic Biochips

Debraj Kundu, Sudip Roy, *Member, IEEE*, Sukanta Bhattacharjee, *Member, IEEE*, Sohini Saha, Krishnendu Chakrabarty, *Fellow, IEEE*, Partha P. Chakrabarti, *Senior Member, IEEE* and Bhargab B. Bhattacharya, *Fellow, IEEE*

***Abstract*—Microfluidic biochips have recently em significant promise and versatility in automating a biochemical protocols on a tiny chip. Sample preparat involves mixing of fluids with a specified target ra minuscule scale, is an essential component of these Algorithms that optimize on-chip sample-preparatio time are closely intertwined with the underlying mix mixing sequence, and fluidic architecture. Although mixing models have been studied in the literature, their the dynamics of mixing steps is hitherto not fully und this paper, we show that various mixing models can be in the light of prime factorization of integers thus e a connection among mixing algorithms, chip architec performance. This insight has led to the developm proposed *factorization-based dilution algorithm* (*FacD* ering a generalized mixing model suitable for micro dot-array (MEDA) biochips. It further leads to *tar oriented dilution algorithm* (*TVODA*) to cater to user for an output with a given volume. We formulate the op problem on the fabric of the Satisfiability Modulo Theory (SMT) while determining mixing sequences. Simulation results on a large number of test-cases reveal that *FacDA* and *TVODA* outperform the state-of-the-art dilution algorithms for MEDA biochips with respect to reactant cost, mixing time, and waste production.**

I. Introduction

Microfluidic biochips or lab-on-a-chips (LoCs) have paved the way to the miniaturization of the biochemical protocols (bio-protocols) on a tiny device [2]–[4]. These chips integrate multiple fluidic operations (dispensing, mixing, detection, etc.) for reliable and cost-effective implementation of bio-protocols. LoCs have brought a paradigm shift in several biochemical applications such as point-of-care diagnostics [5], genomics [6, 7], drug design [8], and biomedical research [9, 10].

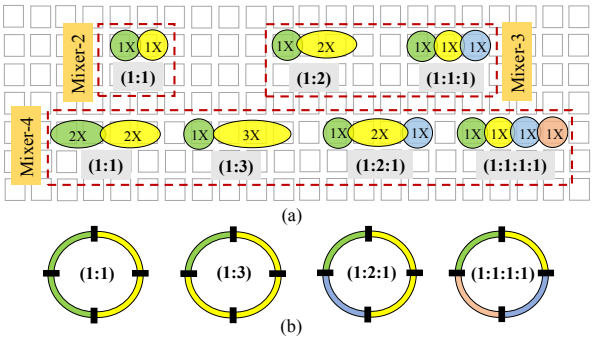

Fig. 1: Schematic view of various mixing models realized in (a) a MEDA biochip with Mixer-2, Mixer-3 and Mixer-4. (b) a 4-segment rotary mixer (RMixer-4).

Several platforms have been proposed such as continuous-flow microfluidic biochips (CFMBs) and digital microfluidic biochips (DMFBs). CFMBs manipulate fluid flow through a network of micro-channels by actuating the micro-valves [2]. DMFBs can manipulate discrete fluid droplets on a 2D-array of electrodes using electrical actuations [11, 12]. Recent advances in fabrication technology for DMFBs have led the development of micro-electrode-dot-array (MEDA) [13]. As shown in Fig. 1(a), a MEDA-based DMFB (referred as MEDA biochip in this paper) comprises of a sea of micro-electrodes with integrated sensors [13, 14].

Sample preparation is a fundamental preprocessing step of many bio-protocols, where the task is to mix two (in case of dilution) or more (in case of mixing) biochemical reagents (fluids) in a volumetric ratio. For DMFBs, many sample preparation algorithms [15]–[23] have been reported. In DMFB we can mix two different fluids by taking only two unit-volume of each, which is modelled as $1:1$ and implemented with Mixer-2 as shown in Fig. 1(a). In contrast, several sample preparation algorithms for CFMBs have also been reported [24, 25], which exploit flexible mixing models supported by a rotary mixer [26]. In an M-segment rotary mixer denoted as RMixer-M, each supported mixing model has an one-to-one correspondence with an unordered integer partition of the integer M into two or more parts. For example, the possible integer partitions of 4 are $2+2, 1+3, 2+1+1$ and $1+1+1+1$, and the corresponding mixing models supported by RMixer-4 are $(1:1)$, $(1:3)$, $(1:2:1)$, and $(1:1:1:1)$, respectively as shown in Fig. 1(b).

MEDA biochips offer more granularity over the shape and

A preliminary version of this paper has appeared in the proceedings of ASPDAC 2019 [1]. This work of D. Kundu and S. Roy was supported by SERB, Govt. of India under grant no.: ECR/2016/001921. The work of K. Chakrabarty was supported in part by the US National Science Foundation under grants CCF-1702596 and ECCS-1914796. The work of B. B. Bhattacharya was supported, in part, from the grant provided by INAE Chair Professorship, and from a special PPEC-funded grant to Nanotechnology Research Triangle provided by Indian Statistical Institute, Kolkata (2012-2018).

D. Kundu and S. Roy are with the Department of Computer Science and Engineering, Indian Institute of Technology Roorkee, Roorkee, India, Email: dkundu@cs.iitr.ac.in; sudip.roy@cs.iitr.ac.in.

S. Bhattacharjee is with the Department of Computer Science and Engineering, Indian Institute of Technology Guwahati, India, E-mail: sukantab@iitg.ac.in.

S. Saha is with the Department of Information Technology, Indian Institute of Engineering Science and Technology, Shibpur, India, E-mail: sohinisaha996@gmail.com.

K. Chakrabarty is with the Department of Electrical and Computer Engineering, Duke University, Durham, USA, E-mail: krish@ee.duke.edu.

P. P. Chakrabarti and B. B. Bhattacharya are with the Department of Computer Science and Engineering, Indian Institute of Technology Kharagpur, Kharagpur, India, Email: {ppchak, bhargab}@cse.iitkgp.ac.in.

size of the droplets and more flexibility o tions [13]. Let M denotes the maximum be mixed at a time on a MEDA biochip. the mixing-volume constraint where the pos a mixture produced by Mixer-M on a ME $(M, M-1, \cdots, 2)$ [27, 28]. For Mixer-M mixing models can be abstracted as the i of $M, M-1, \cdots, 2$. As shown in Fig. 1 $(M = 4)$, the supported mixing models are $(1:1:1)$, $(1:3)$, $(1:2:1)$, and $(1$ This opens a new problem, where the ques sample preparation method that can exploit a supported by a MEDA biochip. Unlike DMFI and-split operations on MEDA are referred separate" steps since separation of mixed flu components is supported by such architecture in this paper, we refer this mix-and-separate st step.

Two algorithms for automated sample preparation on MEDA biochips have been reported in the recent past. Li *et al.* proposed a dilution algorithm for MEDA biochips known as *weighted sample preparation method* (*WSPM*) [27] that uses only $(m:n)$ mixing model ($(m:n) \subset$ Mixer-M) in each step. Therefore, it can use only a subset of mixing models supported by MEDA biochips. Recently, Liang *et al.* proposed a top-down approach called *multiple-reactant cost minimization* (*MRCM*) [28] to determine a mixing tree. *MRCM* exploits possible mixing models supported by a Mixer-M, though the volume obtained in a mixing step is not shared with any of its ancestors except its parent mixing step.

In this paper, we present a new dilution algorithm for MEDA biochip called *division-by-factor method* (*DFM*) to generate a skewed dilution graph which exploits all the mixing models of Mixer-M. We present *factorization-based dilution algorithm* (*FacDA*), which uses the structure of the dilution tree determined by *DFM* and models a dilution graph that attempts to maximize sharing edges. We deploy a satisfiability modulo theory (SMT) based solver to implement FacDA for generating a dilution graph/tree that reduces the amount of sample usage. For dilution of a fluid with any given target volume, we further extend *FacDA* to propose *target volume oriented dilution algorithm* (*TVODA*). In *TVODA*, the underlying optimization problem is modeled as an SMT formulation. This determines a dilution graph that can be tuned to reduce the number of mixing steps, the amount of sample usage and total wastage significantly.

The remainder of the paper is organized as follows. Sec. II describes preliminaries and prior work. Sec. III explains the proposed approach, *FacDA*. Sec. IV presents *TVODA* and Sec. V describes the optimization criteria and scopes for both *FacDA* and *TVODA*. Sec. VI reports simulation results for performance evaluation. Finally, Sec. VII concludes the paper.

II. Preliminaries and Prior Work

This section presents the basics of dilution and MEDA biochips and related prior work on sample preparation.

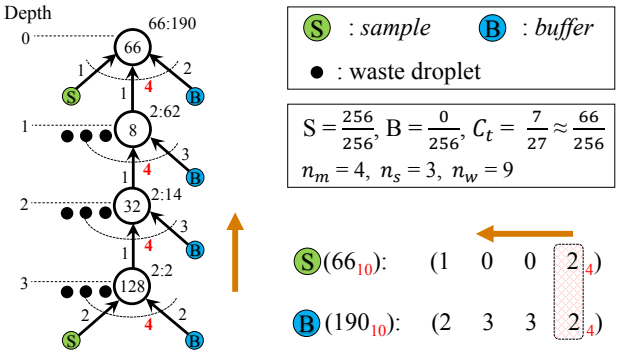

Fig. 2: Dilution tree for $C_t = \frac{7}{27}$, $M = 4$ and $\epsilon = 0.005$, using *NWayMix* [24].

A. Basics of Dilution

Dilution is a special case of sample preparation, where only two reagents (*sample* and *buffer*) are mixed in a desired volumetric ratio. An automated dilution problem consists of a sequence of mixing steps is represented as a directed acyclic graph called dilution tree/graph, where each node represents a mixing step. The inputs of a dilution problem are: (1) target ratio, *sample* : *buffer* $= x : y$, which can also be represented as a target concentration factor (CF), $C_t = \frac{x}{x+y}$, (2) a set of mixing models corresponding to the mixing volume constraint M, and (3) error-tolerance, where CFs of pure *sample* and *buffer* are 1 and 0, respectively. The CF of a mixing node at depth i is calculated as $CF_i = \frac{c_1 \times v_1 + c_2 \times v_2 + \cdots + c_n \times v_n}{v_1 + v_2 + \cdots + v_n}$, for n incoming edges having CF and volume contribution as cjs and v_js, respectively. The volumetric ratio of *sample* and *buffer* in the mixing node at depth i is computed as $X_i : Y_i = CF_i : (1 - CF_i)$, where X_i and Y_i denote the contribution of *sample* and *buffer* in that mixing node. We avoid the fractional representation of the CFs in the figures and represent CF_i with their numerator only. Due to the unavailability of a desired mixing model in a microfluidic platform, a target ratio may require to be transformed into another ratio, which may incur an error in it. Given an error-tolerance ϵ, the transformation procedure of target ratio $x : y$ into $x' : y'$ is demonstrated in **Appendix A**. After performing the ratio transformation, for target ratio $x : y = 7 : 27$ ($C_t = \frac{7}{27}$), $\epsilon = 0.005$ and $M = 4$, the dilution tree determined by *NWayMix* [24] is shown in Fig. 2. The total number of mixing steps (n_m), the total volume of *sample* required (number of *sample* units n_s) and the total volume of waste droplets (number of waste units n_w) for the dilution tree shown in Fig. 2 are 4, 3 and 9, respectively. The following example illustrates the calculation of the CFs at different depths of the dilution tree shown in Fig. 2.

Example 1: The CFs at the mixing nodes from the bottom-most depth are calculated as follows: $CF_3 = \frac{1\times2+0\times2}{2+2} = \frac{2}{4}$ *(written as* $\frac{2}{4} \times 256 = 128$ *in Fig. 2) and* $X_3 : Y_3 = \frac{2}{4} : (1 - \frac{2}{4}) = 2 : 2$. *Similarly,* $CF_2 = \frac{CF_3\times1+0\times3}{4} = \frac{\frac{2}{4}\times1+0\times3}{4} = \frac{2}{16}$ *and* $X_2 : Y_2 = 2 : 14$. *Likewise,* $CF_1 = \frac{\frac{2}{16}\times1+0\times3}{4} = \frac{2}{64}$ *and* $X_1 : Y_1 = 2 : 62$. *Finally, at depth 0,* $CF_0 = \frac{1\times1+\frac{2}{64}\times1+0\times2}{4} = \frac{66}{256}$ *and the corresponding target ratio* $X_0 : Y_0 = 66 : 190$.

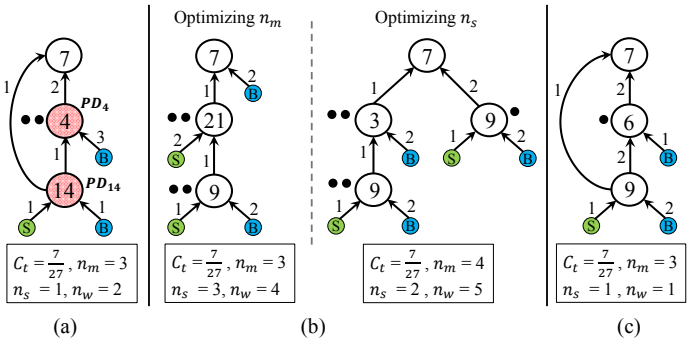

Fig. 4: For $C_t = \frac{7}{27}$, $M = 4$ and $\epsilon = 0.005$, G_D obtained by (a) *WSPM* [27], (b) *MRCM* [28], and (c) *FacDA*.

of 8×8 micro-electrode cell is considered as a mixing region and within it the 4×4 shaded region indicates the merging region. Fig. 3(b) shows three different fluids of 1, 3, and 4 unit volumes, which are to be mixed within an *SAR* based laminar mixer of $M = 8$ using $(1 : 3 : 4)$ mixing model. Fig. 3 depicts four different phases of the corresponding mix-cycle such as merge (Fig. 3(c)), split (Fig. 3(d)), shift (Fig. 3(e)), and merge again (Fig. 3(f)). This kind of mix-operation decreases the diffusion length between the fluids by exponentially increasing the interfacial surface area (shown in Fig. 3(f)), which accelerates the mix-operation in MEDA biochips compared to that in DMFBs [13].

C. Sample Preparation on MEDA Biochips: Prior Work

LoC-based sample preparation algorithms consider three different optimization objectives: minimization of (1) the number of mixing steps, (2) the consumption of valuable reagents, and (3) the amount of overall wastage. Li *et al.* proposed *weighted sample preparation method (WSPM)* [27] for dilution, which considers reagent saving as the primary objective. *WSPM* initially generates a set of primary droplets (*PD*s) through a sequence of dilution operations using only $(m : n)$ mixing model and always taking one of the i as *buffer*. The main purpose of the primary dilution opera is to minimize the *sample* usage. For a mixer of size 4 ($M = 4$), *WSPM* can use only $(1 : 1), (1 : 2)$ and $(1$ mixing models out of six possible mixing models show Fig. 1(a) for a Mixer-4. After constructing an estimated table for the *PD*s and their intermediate fluids, *WSPM* ad a top-down approach to generate the initial dilution tree u $(m : n)$ mixing models, in which only the *PD*s appea

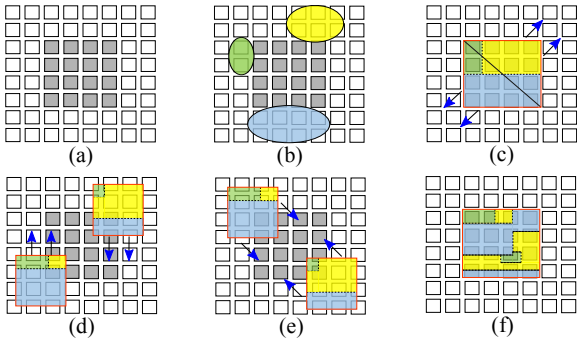

Fig. 3: Schematic view of *SAR* based laminar MEDA m showing different phases of a mix-cycle.

leaf nodes. Finally, the *sample* usage is reduced by sharing of *PD*s in the dilution tree if possible. Using the *PD*s $\frac{14}{27}$ and $\frac{4}{27}$, *WSPM* determines the dilution graph for $C_t = \frac{7}{27}$ as shown in Fig. 4(a). Recently Liang *et al.* proposed a top-down approach for mixing in MEDA (a.k.a. *multiple-reactant cost minimization* (*MRCM*) [28]) that minimizes the usage of the most costly reagent. For a given target ratio, *MRCM* determines the mixing tree by enumerating all possible mixing models using intermediate and/or pure concentrations, and then choosing the mixing model with the minimum usage of the concerned reagent. The same process continues recursively for the set of newly generated intermediate concentrations until all the leaf nodes of the mixing tree have pure reagents. Fig. 4(b) shows two different dilution trees determined by *MRCM* for a target ratio *sample* : *buffer* $= 7 : 20$, where the number of mixing steps and *sample* usage are considered as optimization objectives, respectively.

III. Factorization Based Dilution on MEDA

A. Motivation and Overview

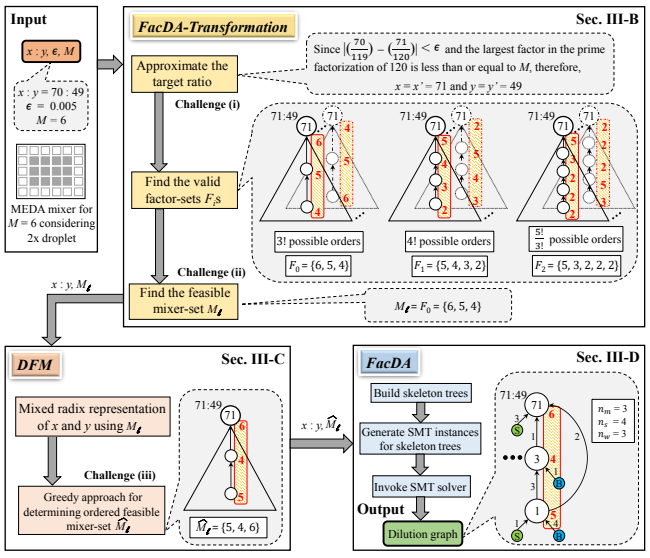

Fig. 5: Flowchart of *FacDA* and number-theoretic challenges.

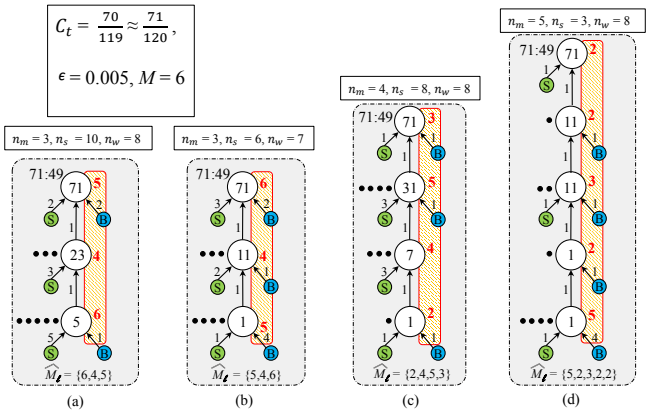

Fig. 6: For $C_t = \frac{70}{119}$ or $x : y = 70 : 49$, with $M = 6$ and $\epsilon = 0.005$, the dilution trees for ordered feasible mixer-set (a) $\widehat{M}_\ell = \{6, 4, 5\}$, (b) $\widehat{M}_\ell = \{5, 4, 6\}$, (c) $\widehat{M}_\ell = \{2, 4, 5, 3\}$ and (d) $\widehat{M}_\ell = \{5, 2, 3, 2, 2\}$.

mixing models and also sharing the intermediate fluids from a mixing node to any of its ancestors for reducing the overall wastage. Figs. 4(a), 4(b) and 4(c) present the comparative values of concerned parameters for the dilution graphs obtained by *WSPM*, *MRCM* and *FacDA* for the same example.

Given a target ratio $x : y$, where $x + y = N$, the basic problem lies in the nature of factors present in the prime factorization of ratio-sum N while approximating the target ratio. The largest composite or prime factor ($\leq M$) from those factors of N determines the mixing area within M, the possible exploitation of the mixing models, and the fluid splitting strategy for Mixer-M. The choice of distinct factors determines the mixing models to be used, and the ordering of these factors determines the performance parameters (n_m, n_s and n_w) of the dilution tree. The chosen integer factorization of the ratio-sum abstracts the mixing models to be used on the given MEDA biochip. Hence, the choice of the ratio-sum while approximating the target ratio, without compromising its accuracy, plays a crucial role in determining the efficient dilution tree. This work is based on this philosophy and more importantly, all previous mixing models considered so far will become special cases of this framework.

Given a target ratio $x : y$, the error-tolerance ϵ, and the mixing volume constraint M, in order to determine the mix-split operations for dilution in a MEDA biochip, there exists some number-theoretic challenges (shown in Fig. 5), i.e., three problems to solve:

(i) choosing the largest prime factor ($\leq M$) while approximating the target ratio within the error tolerance ϵ,

(ii) choosing the number of distinct (prime and/or composite) factors ($\leq M$), and

(iii) choosing the order of those factors.

Fig. 5 depicts the flowchart of the proposed method along with a demonstration of these number theoretic challenges with the help of a problem instance having $x : y = 70 : 49$, $\epsilon = 0.005$ and $M = 6$. For the same problem instance, Fig. 6 presents four possible dilution trees for arbitrary ordering of different feasible factors, where all the dilution trees have the largest factor (6 or 5) within M. Still, the values of n_m, n_s and n_w for those dilution trees vary with the solutions to the challenges discussed above, i.e., choosing the number of distinct factors and their orders. Comparing the dilution trees shown in Fig. 6(a) or Fig. 6(b) with Fig. 6(c) and Fig. 6(d), we can visualize that n_m increases with the increase in the number of distinct factors (challenge (ii)). However, with the same set of feasible factors considered in the dilution trees of Fig. 6(a) and Fig. 6(b), the values of n_s and n_w also vary with different orderings of those factors in the corresponding dilution trees (challenge (iii)).

In this paper, we proposed an approach to solve these problems in three phases. At first, *FacDA-Transformation* (detailed in Sec. III-B) approximates the target ratio (if required) and determines the feasible mixer-set M_ℓ. Second, *DFM* (detailed in Sec. III-C) uses the output of *FacDA-Transformation* to determine the ordered feasible mixer-set $\widehat{M}_\ell$. Third, *FacDA* (detailed in Sec. III-D) is invoked to build a skeleton tree TS corresponding to the dilution tree returned by *DFM*. Then, it generates the SMT instances for a sequence of decision problems using $\widehat{M}_\ell$ and a set of constraints over integers, and finally, *FacDA* utilizes the SMT solver to determine the dilution graph G_D with minimum *sample* requirement.

B. Transformation of Target Ratio

Given the target ratio *sample* : *buffer* $= x : y$, a valid factor-set $F_i = \{f_0, f_1, \cdots, f_{n_i}\}$ is defined as a set of factors of ratio-sum N $(= x + y)$ such that each element of F_i lies within the range of 2 and M, i.e., $2 \leq f_0, f_1, \cdots, f_{n_i} \leq M$. Furthermore, the product of all the elements of F_i must be equals to N, i.e., $\prod_{j=0}^{n_i} f_j = N$. In the proposed approach, the target ratio $x : y$ needs to be transformed, if the ratio-sum $(N = x + y)$ is a prime number greater than the mixing volume constraint M, or N has no valid factor-set. From the list of all valid factor-sets L_M, the least cardinality set is defined as the feasible mixer-set M_ℓ. **Algorithm 1** presents the procedure *FacDA-Transformation*, which is executed in a recursive manner until both the objectives for satisfying the mixing volume constraint (M) and the error-tolerance (ϵ) are met. *FacDA-Transformation* returns the transformed target ratio (if required) and the feasible mixer-set M_ℓ as illustrated in *Example* 2. The elements of M_ℓ determine the mixer size at different depths of the dilution graph to be obtained later.

Algorithm 1: *FacDA-Transformation*$(x : y, \epsilon, M)$

Input: Target ratio *sample* : *buffer* $= x : y$, where $x + y = N$, error-tolerance ϵ, mixing volume constraint M
Output: Transformed ratio $x' : y'$, feasible mixer-set M_ℓ

```
begin
    /* Factorization of N. */
    Obtain the set of all valid factor-sets of N, i.e.,
      L_M = {F_0, F_1, F_2, ..., F_m}, where each factor-set
      F_i = {f_0, f_1, ..., f_{n_i}} such that ∀f_j ∈ F_i, 2 ≤ f_j ≤ M and
      N = ∏_{j=0}^{n_i} f_j;
    if L_M ≠ φ then
        Find the least cardinality set M_ℓ from L_M;
        return (x : y, M_ℓ);
    N' = N + 1; x' = RoundOff((x/(x+y)) · N'); y' = N' − x';
    while |x/N − x'/N'| > ε do
        N' = N + 1; x' = RoundOff((x'/(x'+y')) · N'); y' = N' − x';
    return FacDA-Transformation(x' : y', ε, M);
```

Example 2: Consider a target ratio $\{sample : buffer = 70 : 49\}$*, where target* $CF\ C_t = \frac{70}{119}$*,* $M = 6$ *and* $\epsilon = 0.005$*. Here,* $N = 70 + 49 = 119$ *and its factors are* $17, 7$ *and* 1*. As* M *is less than both* 17 *and* 7 *no valid factor-set can be obtained, i.e.,* $L_M = \phi$ *and we need to transform the target ratio. After increasing the ratio-sum* N *by one we get* $N' = 120$*. The transformed ratio becomes* $x' : y' = 71 : 49$*, which satisfies the error-tolerance, i.e.,* $|(\frac{70}{119}) - (\frac{71}{120})| < \epsilon$*. For* $N' = 120$*, we get* $L_M = \{\{6, 5, 4\}, \{5, 4, 3, 2\}\}$*, i.e,* $F_0 = \{6, 5, 4\}$ *and* $F_1 = \{5, 4, 3, 2\}$*, which implies that* M_ℓ *is* $\{6, 5, 4\}$*.*

C. Division-by-Factor-Method (DFM)

We propose an approach called *division-by-factor-method* (*DFM*), which leverages the support of variable size mixers in MEDA for diluting the *sample* with *buffer*. Given the target ratio $x : y$, the mixing volume constraint M and the error-tolerance ϵ, *DFM* calls *FacDA-Transformation* and obtain a transformed ratio $x : y$ and M_ℓ to determine a dilution tree.

1) Determining a dilution tree using mixed radix representation: Let the cardinality of the feasible mixer-set M_ℓ returned by *FacDA-Transformation* be d, where $M_\ell = \{f_0, f_1, \cdots, f_{d-1}\}$. Then we can use any ordered arrangement of M_ℓ as a mixed radix to represent x and y as d-digit numbers, where $x : y$ is the target ratio returned by *FacDA-Transformation*. Without loss of generality, we assume that the radix at position i is f_i, for $i = 0, 1, \cdots, d-1$ and $\{f_0, f_1, \cdots, f_{d-1}\}$ is referred as the mixed radix vector. We use the conventional division method to represent x and y as two d-digit numbers in mixed radix $\{f_0, f_1, \cdots, f_{d-1}\}$. Let x is represented as $x_{d-1}x_{d-2}\cdots x_1x_0$ in mixed radix, where f_i is used as the radix at position i for $i = 0, 1, \cdots, d-1$. Therefore, the decimal value of x can be calculated as $\left(\sum_{i=1}^{d-1}(\prod_{j=0}^{i-1} f_j)x_i\right) + x_0$. Similarly, the decimal value of y can also be calculated. Fig. 7(a) depicts the generic representations of x and y in d-digit mixed radix vector $\{f_0, f_1, \cdots, f_{d-1}\}$, stored in a table called decomposition-table. In the decomposition-table, the first column shows the mixed radix vector, and the second and third column contains x and y in mixed radix $\{f_0, f_1, \cdots, f_{d-1}\}$, i.e., $x_{d-1}x_{d-2}\cdots x_1x_0$ and $y_{d-1}y_{d-2}\cdots y_1y_0$, respectively. We can determine the dilution tree of height d in a bottom-up approach by scanning the elements of the first three columns of the decomposition-table in a top-down order, where f_i denotes the size of the mixer and x_i (y_i) determines the volume of pure *sample* (*buffer*) used in the mixing node at depth $(d-1-i)$. Alternately at depth i of the dilution tree, the size of the mixer and the volume of pure *sample* (*buffer*) are represented as f_{d-1-i} and x_{d-1-i} (y_{d-1-i}), respectively.

Note that, a mixing node of the obtained dilution tree shares one-unit volume, only to its parent mixing node.

The total number of mixing steps n_m, the number of *sample* units n_s and the number of waste units n_w of the dilution tree can be calculated directly from the decomposition-table as shown in Fig. 7(a). The following example illustrates the process of determining the dilution tree from the decomposition-table for a given target ratio.

Example 3: Assume that the mixed radix vector corresponding to the feasible mixer-set $M_\ell = \{6, 5, 4\}$ *in Example 2 is* $\{4, 5, 6\}$*. Then,* $x = 71_{10} = (4 \times 5 \times \underline{3}) + (4 \times \underline{2}) + \underline{3}$ *and* x *is represented as* 323 *in mixed radix* $\{4, 5, 6\}$*. Similarly,* $y = 49 = (4 \times 5 \times \underline{2}) + (4 \times \underline{2}) + \underline{1}$ *and* y *is represented as* 221 *in mixed radix* $\{4, 5, 6\}$*. Scanning the values of mixed radix vector,* x_i *and* y_i*, in a top-down order we can determine the corresponding dilution tree in a bottom-up approach as shown in Fig. 7(b).*

2) Determining the ordering of feasible mixer-set (M_ℓ)*:* If M_ℓ of cardinality d is considered as a d-digit radix vector, then $d!$ number of dilution trees can be realised corresponding to $d!$ ordered arrangements of M_ℓ. Each of these dilution trees of height d is different and may have different values of n_s and n_w. Thus, for choosing an ordered arrangement of M_ℓ (referred as $\widehat{M_\ell}$) to determine a suitable dilution tree, we adopt the following greedy-approach. In order to get the maximum volume of the target ratio, initially the largest element of M_ℓ is selected as the last, i.e., the $(d-1)^{\text{th}}$ element of $\widehat{M_\ell}$. Next, in order to determine all the other elements of $\widehat{M_\ell}$, we build a function that performs the following two steps:

(i) computing the volume of pure *sample* (x_{d-1-i}) required at depth i for each element of M_ℓ, which are not yet selected for $\widehat{M_\ell}$, and

(ii) selecting an element of M_ℓ from step (i) as the $(d-1-i)^{\text{th}}$ element of $\widehat{M_\ell}$, which requires the least x_{d-1-i}. We recursively call the said function, starting from depth $d-1$ to depth 1 sequentially, to determine $\widehat{M_\ell}$. The estimation for determining $\widehat{M_\ell}$ returned by *DFM* is in the $O(|M_\ell|^2)$.

This greedy approach is explained with *Example*. 4. The *DFM* comprises of two methods explained above in Sec. III-C1 and Sec. III-C2 to determine the corresponding dilution tree for the target ratio $x : y$ using $\widehat{M_\ell}$.

Example 4: Considering Example 2, from the feasible mixer-set $M_\ell = \{6, 4, 5\}$ *returned by FacDA-Transformation we can generate* $3!$ *ordered arrangements of mixed radix vector as* $\{4, 5, 6\}, \{4, 6, 5\}, \{5, 4, 6\}, \{5, 6, 4\}, \{6, 4, 5\}$ *and* $\{6, 5, 4\}$*. DFM determines* $\widehat{M_\ell}$ *as follows: initially the largest element of* $M_\ell = \{6, 4, 5\}$*, i.e., 6 is inserted in the* 2^{nd} *position of* $\widehat{M_\ell}$*, so* $\widehat{M_\ell} = \{\_, \_, 6\}$*. Since* x_0 *for* 5 *(=1) in Fig. 7(c) is lesser than* x_0 *for* 4 *(=3) in Fig. 7(b), 5 is inserted in the* 0^{th} *position of* $\widehat{M_\ell}$*, so* $\widehat{M_\ell} = \{5, \_, 6\}$*. Next, as 4 is the remaining element of* M_ℓ *which has not yet been selected, 4 is inserted in the* 1^{st} *position of* $\widehat{M_\ell}$*, so* $\widehat{M_\ell} = \{5, 4, 6\}$ *and the corresponding dilution tree is shown in Fig. 7(c).*

D. Factorization-based Dilution Algorithm (FacDA)

DFM determines a skewed dilution tree, where each mixing node of size f_{d-1-i} shares only one unit volume to their parent node. As a result, $(f_{d-1-i} - 1)$ unit volume of waste is generated at depth i of a dilution tree. In order to reduce these wastage, we consider sharing edges from a mixing node to all of its ancestors. Similar to the dilution tree determined by *DFM*, we construct an unweighted tree with all the valid sharing edges, and two edges for pure *sample* and *buffer* corresponding to each mixing node. This tree is coined as skeleton tree TS, which uses the same ordered feasible mixer-set $\widehat{M_\ell}$ as determined by *DFM*. The different components of a TS are the mixing nodes, the valid sharing edges and the

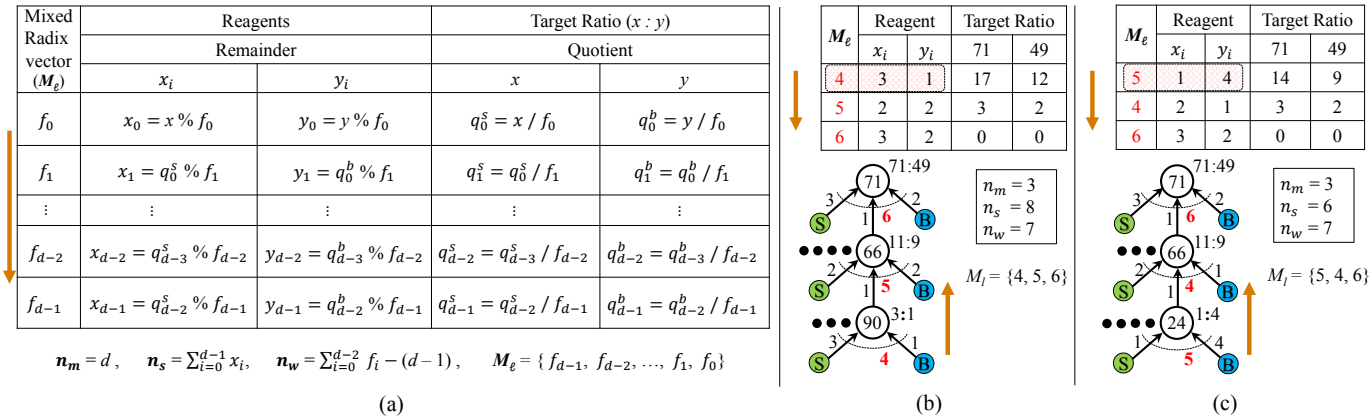

Fig. 7: (a) Decomposition-table for a target ratio $x : y$ and mixed radix vector $\{f_0, f_1, \cdots, f_{d-1}\}$, and closed-form formulae for estimating n_m, n_s, n_w and M_ℓ from the table. For target ratio $x : y = 71 : 49$ and $M = 6$, decomposition-table and dilution tree, (b) if $M_\ell = \{4, 5, 6\}$, and (c) if $M_\ell = \{5, 4, 6\}$.

edges for pure *sample* and pure *buffer*, as shown in Fig. 8(a). In Fig. 8(a), all the dashed edges represent the edges which are not considered in *DFM*. The variables corresponding to mix-i of TS are X_i, Y_i, x_{d-1-i}, y_{d-1-i}, and all the valid sharing edges from mix-i, i.e., $w_{i,j}$s, where $j = \{i-1, i-2, \cdots, 0\}$, to mix-$j$ are as follows (Fig. 8(b)):

- $X_i : Y_i$: the ratio of *sample* and *buffer* at depth i.
- $w_{i,j}$: volume of the fluid shared from mix-i at depth i to mix-j at depth j.
- x_{d-1-i}, y_{d-1-i}: volume of *sample* and *buffer* used in mix-i at depth i, respectively.

Next, we model the problem of dilution by defining integer variables corresponding to each variable of mix-i, $i = \{d-1, d-2, \cdots, 0\}$, of a TS and build a set of linear and non-linear constraints over those variables. Some key properties of a TS are presented as the following observations, and illustrated with *Example* 5 and *Example* 6 for the dilution graph shown in Fig. 8(e).

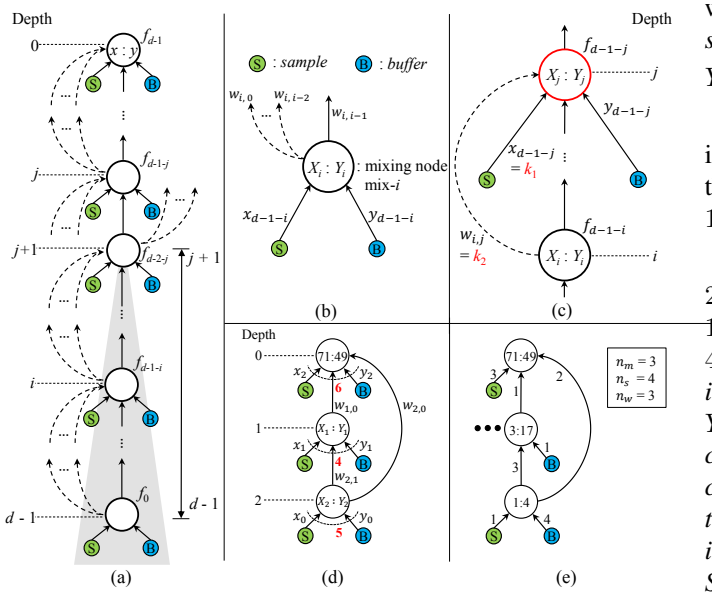

Fig. 8: (a) Skeleton tree TS of height d with all of its components. (b) Variables corresponding to a mixing node mix-i of TS. (c) Sharing of k_1 unit volume of pure *sample* and k_2 unit volume from mix-i to mix-j of TS. For $x : y = 71 : 49$ and $M = 6$, (d) TS and (e) G_D determined by *FacDA*.

Observation 1: If k_1 unit volume of pure *sample* is used in mix-j at depth j of TS, i.e., $x_{d-1-j} = k_1$ (Fig. 8(c)), where $0 \leq j \leq (d-1)$, then the contribution of *sample* in $X_j : Y_j$ at mix-j is $k_1 \prod_{p=j+1}^{d-1} f_{d-1-p}$.

*Example 5: For the dilution graph of Fig. 8(e), in mix-*0*, the contribution of sample is* $x_2 \times f_0 \times f_1 = 3 \times 5 \times 4 = 60$*, and the contribution of buffer is* $y_2 \times f_0 \times f_0 = 0 \times 5 \times 4 = 0$*. Similarly, in mix-*1*, the contribution of sample is* $x_1 \times f_0 = 0 \times 5 = 0$ *and the contribution of buffer is* $y_1 \times f_0 = 1 \times 5 = 5$*. Finally, in mix-*2*, the contribution of sample is* $x_0 = 1$ *and the contribution of pure buffer is* $y_0 = 4$*.*

Observation 2: If k_2 unit volume from mix-i at depth i is shared to mix-j at depth j of TS, i.e., $w_{i,j} = k_2$ (Fig. 8(c)), where $0 \leq j < i \leq (d-1)$, then the contributions of *sample* and *buffer* in $X_j : Y_j$ are $X_i k_2 \prod_{p=j+1}^{i-1} f_{d-1-p}$ and $Y_i k_2 \prod_{p=j+1}^{i-1} f_{d-1-p}$, respectively.

In order to compute the contributions of *sample* and *buffer* in mix-j from all the mixing nodes below it, we have to add the corresponding contributions of all $w_{p,j}$s, where $p = \{j+1, j+2, \cdots, d-1\}$.

*Example 6: In the dilution graph of Fig. 8(e), from mix-*2 *to mix-*0*, the contribution of sample is* $X_2 \times w_{2,0} \times f_1 = 1 \times 2 \times 4 = 8$*, and the contribution of buffer is* $Y_2 \times w_{2,0} \times f_1 = 4 \times 2 \times 4 = 32$*. From mix-*2 *to mix-*1*, the contribution of sample is* $X_2 \times w_{2,1} = 1 \times 3 = 3$*, and the contribution of buffer is* $Y_2 \times w_{2,1} = 4 \times 3 = 12$*. Similarly, from mix-*1 *to mix-*0*, the contribution of sample is* $X_1 \times w_{1,0} = 1 \times 3 = 3$*, and the contribution of buffer is* $Y_1 \times w_{1,0} = 1 \times 17 = 17$*. As a result, the total contribution of sample in mix-*0 *from mix-*1 *and mix-*2 *is* $X_2 \times w_{2,0} \times f_1 + X_1 \times w_{1,0} = 1 \times 2 \times 4 + 3 \times 1 = 8 + 3 = 11$*. Similarly, the total contribution of buffer in mix-*0 *from mix-*1 *and mix-*2 *is* $Y_2 \times w_{2,0} \times f_1 + Y_1 \times w_{1,0} = 2 \times 4 \times 4 + 17 \times 1 = 32 + 17 = 49$*.*

The proofs of **Observation 1** and **Observation 2** are detailed in **Appendix B1** and **Appendix B2**, respectively. From **Observation 1** and **Observation 2**, the total contributions of *sample*

and *buffer* in $X_j : Y_j$ at depth j of a TS are computed as

$$\left(x_{d-1-j}\prod_{q=j+1}^{d-1} f_{d-1-q} + \sum_{p=j+1}^{d-1}(X_p w_{p,j}\prod_{q=j+1}^{p-1} f_{d-1-q})\right) : \left(y_{d-1-j}\prod_{q=j+1}^{d-1} f_{d-1-q} + \sum_{p=j+1}^{d-1}(Y_p w_{p,j}\prod_{q=j+1}^{p-1} f_{d-1-q})\right).$$

The validation of the contributions mentioned in **Observation 1** and **Observation 2** for the G_D shown in Fig. 8(e) is demonstrated in the following example.

Example 7: For the G_D shown in Fig. 8(e), we can calculate the CF at depth 0 of TS using the formula explained in Sec. II-A as $\frac{3+(\frac{1}{5}\times 2+\frac{3}{20}\times 1)}{6} = \frac{71}{120}$, *i.e.,* $X_0 : Y_0 = \frac{71}{120} : (1-\frac{71}{120}) = 71:49$. *In order to validate our observations, we derive* $X_0 : Y_0$ *as* $X_0 : Y_0 = (x_2 \times f_0 \times f_1 + X_2 \times w_{2,0} \times f_1 + X_1 \times w_{1,0}) :$ [illegible] $5\times 4+1\times 2\times$

Now, we als
straints with

- As the
  f_{d-1-j},
  buffer)
  f_{d-1-j},

  x_{d-1-}

- As the
  f_{d-1-j},
  its ance

- The variables shown in Fig. 8(b) must satisfy

$$X_i + Y_i = \prod_{p=i}^{d-1} f_{d-1-p},$$
$$0 \le w_{i,j} \le f_{d-1-j} - 1,$$
$$0 \le x_{d-1-i} \le f_{d-1-i} - 1, \text{ and}$$
$$0 \le y_{d-1-i} \le f_{d-1-i} - 1,$$
$$\text{where } 0 \le j < i \le (d-1).$$

Finally, we add these constraints and invoke the SMT solver [29] by calling the function checkSAT() to generate a satisfiable assignment of the variables in order to determine a dilution graph G_D, where the total *sample* usage n_s is minimized. This procedure is referred as *FacDA* and the corresponding pseudo-code is written as **Algorithm 2**. After generating the set of linear and non-linear equations for the

Algorithm

Input: Target r
constrai
Output: Diluti
1 **begin**
2 Obtain th
$\widehat{M_\ell}$ by
/* Line
in S
3 S = SMT
$d = |\widehat{M}$
4 *sample_u*
stor
usec
5 $S' = S \bigwedge (\sum_{i=0}^{d-1} x_i ==$ *sample_unit*$)$;
6 checkSAT(S'); /* checkSAT(S') checks for a satisfiable assignment of the variables in S'. */
7 **while** S' *is unsatisfiable* **do**
8 *sample_unit* = *sample_unit* + 1;
9 $S' = S \bigwedge (\sum_{i=0}^{d-1} x_i ==$ *sample_unit*$)$;
10 checkSAT(S');
11 Obtain dilution graph G_D from the satisfiable assignments of S';
12 **return** Dilution graph G_D;

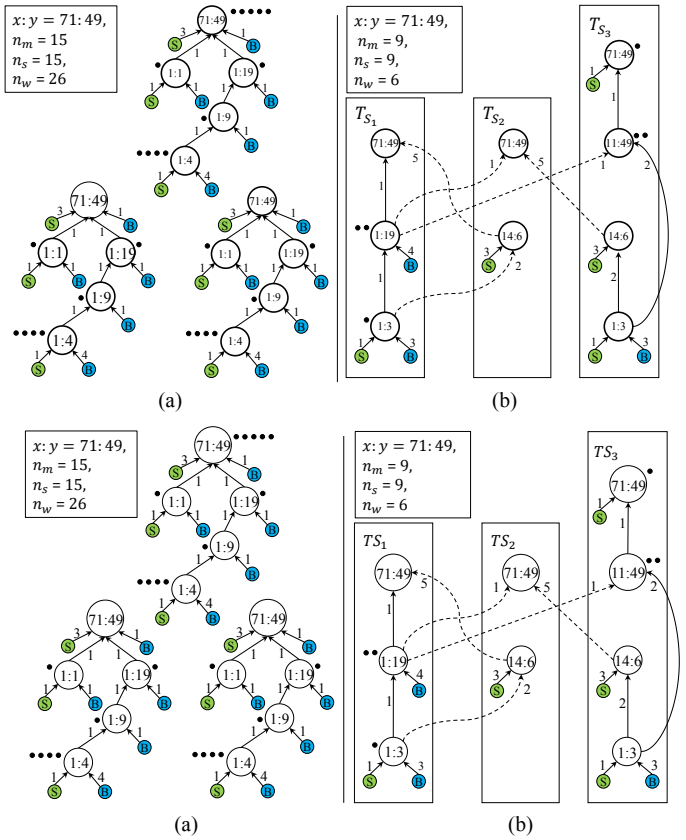

Fig. 9: For target ratio $x : y = 71 : 49$, $M = 6$ and $V_t = 13$, G_D obtained by (a) *MRCM* [28] and (b) *TVODA*.

A. Problem Formulation

The problem of determining the dilution graph producing the target volume of a target ratio can be formulated as follows:
Input: Target ratio *sample* : *buffer* $= x : y$, target volume V_t and mixing volume constraint M.
Output: A dilution graph G_D, which produces V_t unit volume of the desired target ratio.

Objectives: To reuse the intermediate fluids efficiently such that the number of sample units n_s is minimized.

B. Target Volume Oriented Dilution Algorithm (TVODA)

The process of determining the dilution graph G_D using *TVODA* consists of two phases:
(1) construction of a forest of skeleton trees to ensure that the target volume V_t is satisfied, and
(2) determining a dilution graph G_D for V_t by realizing a satisfiable condition of a set of constraints using SMT solver.

1) Construction of skeleton forest: In the first phase of *TVODA*, we implement a greedy strategy to build a forest of skeleton trees such that summation of the mixer size of their root mixing nodes satisfies V_t. Unlike *FacDA*, here we decide the ordering of feasible mixer-set of each skeleton trees in such a way that the number of inter-skeleton sharing edges among the TSs increases. The condition for the validity of a sharing edge between any two skeleton trees TS_m and TS_n primarily depends on the size of each mixer from bottom-most depth to the root node and the ordering of the feasible mixer-set of both the skeleton trees. For $x : y = 71 : 49, M = 6$ and $V_t = 8$, F_{TS} of two skeleton trees TS_1 and TS_2 are shown in Fig. 10(a). For an arbitrary ordered feasible mixer-sets $\widehat{M}^1_\ell = \{4, 5, 6^*\}$ and $\widehat{M}^2_\ell = \{3, 4, 5, 2^*\}$, a valid (check marked) and an invalid (cross marked) inter-skeleton sharing edge between TS_1 and TS_2 are shown in Fig. 10(a). The condition for an inter-skeleton sharing edge to be valid is detailed in the Sec. IV-B2. If we consider any arbitrary ordering of the elements of M_ℓs, then we have to individually check the validity of all possible inter-skeleton sharing edges. However, if any two skeleton trees TS_m and TS_n have k length of common mixer sizes from their bottom-most depths, then there is no need for checking the validity of inter-skeleton sharing edges from those k mixing nodes between TS_m and TS_n. Determining the ordered feasible mixer-sets of the TS for the dilution problem mentioned in Fig. 9 is illustrated in **Appendix C1**.

The number of skeleton trees for a given V_t is in the $O(\varphi)$, where φ is the cardinality of the factor-set of N, where all the elements are $\leq M$. Moreover the maximum number of sharing edges among the skeleton trees is in the $O(\xi \times \psi)$, where ξ implies the maximum number of *TS*s having same $\widehat{M}_\ell$s and ψ is the cardinality of $\widehat{M}^i_\ell$.

2) Formal modelling for TVODA: In *TVODA*, we reuse the intermediate fluids not only within a particular skeleton tree (intra-skeleton) but also among the skeleton trees (inter-skeleton) of F_{TS} and produce an efficient dilution graph in terms of the concerned parameters. The variables corresponding to the mixing node mix-$_i^m$ at depth i of TS_m are X^m_i, Y^m_i, $x^m_{d_m-1-i}$, $y^m_{d_m-1-i}$, and all the valid sharing edges. Descriptions of the variables determining different components of mix-$_i^n$ of TS_n are as follows (Fig. 10(b)):

- $X^m_i : Y^m_i$: the ratio of *sample* and *buffer* at depth i of m^{th} skeleton tree TS_m.
- $w^{m,n}_{i,j}$: the volume of fluid shared from the mixing node mix-$_i^m$ at depth i of TS_m to the mixing node mix-$_j^n$ at depth j of TS_n, represented as weights of inter-skeleton edges
- $w^m_{r,i}$: the volume of the fluid shared from the mixing node mix-$_r^m$ at depth r to the mixing node mix-$_i^m$ at depth i of TS_m, represented as weights of intra-skeleton edges
- $x^m_{d_m-1-i}$ and $y^m_{d_m-1-i}$: the volumes of *sample* and *buffer* used in mixing node mix-$_i^m$ at depth i of TS_m, respectively.
- P^m_i: the product of the mixer sizes corresponding to the mixing nodes of TS_m from depth $d_m - 1$ to i, i.e., $\prod_{q=i}^{d_m-1} f^m_{d_m-1-q}$.

The contributions of *sample* and *buffer* from mix-$_i^m$ to mix-$_j^n$ is written as the following observation.

Observation 3: If k_3 unit volume from mix-$_i^m$ at depth i of TS_m is shared to mix-$_j^n$ at depth j of TS_n, i.e., $w^{m,n}_{i,j} = k_3$ (Fig. 10(c)), then the contributions of *sample* and *buffer* in $X^n_j : Y^n_j$ at mix-$_j^n$ from $X^m_i : Y^m_i$ at mix-$_i^m$ are $X^m_i k_3 \frac{P^n_{j+1}}{P^m_i}$ and $Y^m_i k_3 \frac{P^n_{j+1}}{P^m_i}$, respectively.

Checking the validity of inter-skeleton sharing edges in F_{TS} is a crucial task as it contributes the maximum number of variables to the equations and constraints to the SMT instance [29]. An inter-skeleton sharing edge $w^{m,n}_{i,j}$ is valid, iff $(P^n_{j+1} \mod P^m_i) = 0$, i.e., P^m_i is a factor of P^n_{j+1}. According to this validity condition of inter-skeleton edges, it is implied that if $w^{m,n}_{i,j}$ is valid, then $\forall p, w^{m,n}_{i,p}$ are also valid edges, where $0 \leq p \leq j-1$. Consequently, there is a considerable increment in the number of variables fed into the SMT solver, which increase the computation time and slows down the process. Hence, in order to speed-up the process we further restrict the validity condition and state an inter-skeleton sharing edge $w^{m,n}_{i,j}$ is valid, iff $P^n_{j+1} = P^m_i$. The F_{TS} for the G_D illustrated in Fig. 9(b) with all the valid sharing edges is shown in Fig. 10(d). According to this new validity condition for inter-skeleton edges, $\frac{P^n_{j+1}}{P^m_i} = 1$. Hence, the contributions of *sample* and *buffer* in $X^n_j : Y^n_j$ as discussed in **Observation 3** is simplified as $X^m_i k_3$ and $Y^m_i k_3$, respectively. According to **Observation 3**, for the dilution graph shown in Fig. 9(b), the contributions of inter-skeleton edges in the mixing nodes of TS_2 are illustrated with the following example.

Example 8: The contribution of sample from mix-$_2^1$ to mix-$_1^2$ is $X^1_2 \times w^{1,2}_{2,1} \times \frac{P^2_2}{P^1_2} = 1 \times 2 \times 1 = 2$*, and the contribution of buffer from mix-$_2^1$ to mix-$_1^2$ is* $Y^1_2 \times w^{1,2}_{2,1} \times \frac{P^2_2}{P^1_2} = 3 \times 2 \times 1 = 6$*. Furthermore, the total contribution of sample from mix-$_1^1$ and mix-$_2^3$ to mix-$_0^2$ is* $(X^1_1 \times w^{1,2}_{1,0} \times \frac{P^2_1}{P^1_1}) + (X^3_2 \times w^{3,2}_{2,0} \times \frac{P^2_1}{P^3_2}) = 1 \times 1 \times 1 + 14 \times 5 \times 1 = 71$*, and the total contribution of buffer from mix-$_1^1$ and mix-$_2^3$ to mix-$_0^2$ is* $(Y^1_1 \times w^{1,2}_{1,0} \times \frac{P^2_1}{P^1_1}) + (Y^3_2 \times w^{3,2}_{2,0} \times \frac{P^2_1}{P^3_2}) = 19 \times 1 \times 1 + 6 \times 5 \times 1 = 49$.

The proof of **Observation 3** is mentioned in **Appendix C2**.

Combining the contributions discussed in **Observation 1**, **Observation 2** and **Observation 3**, the desired ratio at depth

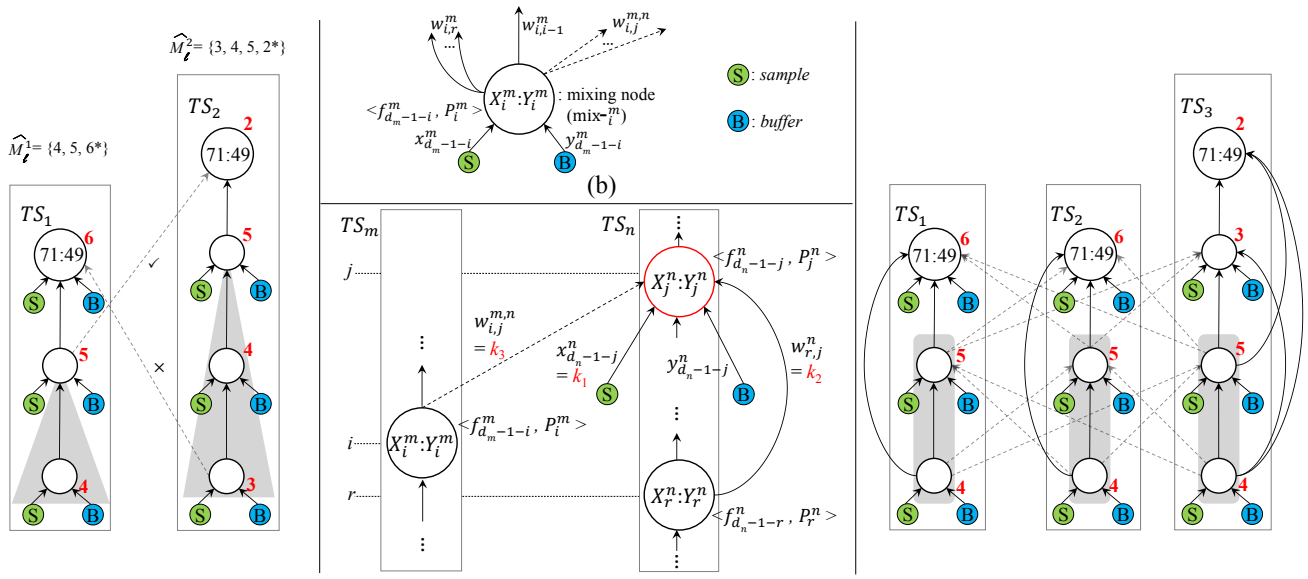

Fig. 10: (a) A valid and an invalid sharing edge between two skeleton trees. (b) Variables corresponding to the components of mixing node mix-$_i^m$ in TS_m. (c) Volume contributions k_1, k_2 and k_3 in mix-$_j^n$ from pure *sample*, mix-$_r^n$ and mix-$_i^m$, respectively. (d) For target ratio $x : y = 71 : 49$, $M = 6$ and $V_t = 13$, the sharing edges in F_{TS} considered by *TVODA*.

j of the n^{th} skeleton TS_n, i.e., $X_j^n : Y_j^n$ can be written as

$$\Bigg(\underbrace{x^n_{d_n-1-j} \prod_{q=j+1}^{d_n-1} f^n_{d_n-1-q}}_{\text{pure } \textit{sample} \text{ contribution}} + \underbrace{\sum_{p=j+1}^{d_n-1} \Big(X^n_p w^n_{p,j} \prod_{q=j+1}^{p-1} f^n_{d_n-1-q} \Big)}_{\text{intra-skeleton contribution}} + \underbrace{\sum_{\forall TS_k \in F_{TS} \mid k \neq n,\ P_i^k = P^n_{j+1}} X_i^k w^{k,n}_{i,j}}_{\text{inter-skeleton contribution}} \Bigg) :$$

$$\Bigg(\underbrace{y^n_{d_n-1-j} \prod_{q=j+1}^{d_n-1} f^n_{d_n-1-q}}_{\text{pure } \textit{buffer} \text{ contribution}} + \underbrace{\sum_{p=j+1}^{d_n-1} \Big(Y^n_p w^n_{p,j} \prod_{q=j+1}^{p-1} f^n_{d_n-1-q} \Big)}_{\text{intra-skeleton contribution}} + \underbrace{\sum_{\forall TS_k \in F_{TS} \mid k \neq n,\ P_i^k = P^n_{j+1}} Y_i^k w^{k,n}_{i,j}}_{\text{inter-skeleton contribution}} \Bigg) .$$

The validation of the contributions mentioned in **Observation 1**, **Observation 2** and **Observation 3** for the G_D shown in Fig. 9(b) is demonstrated in the following example.

Example 9: Using the formula explained in Sec. II-A, we can calculate the CF at depth 1 of TS_2 shown in Fig. 9(b) as $\frac{(1\times3)+(\frac{1}{4}\times2)}{5} = \frac{14}{20}$, *i.e.,* $X_1^2 : Y_1^2 = \frac{14}{20} : (1 - \frac{14}{20}) = 14 : 6$. *To validate our observations, we derive $X_1^2 : Y_1^2$ as,* $X_1^2 : Y_1^2 = (x_1^2 \times f_0^2) + (X_2^2 \times w_{2,1}^2) + (X_1^2 \times w_{2,1}^1 + X_3^3 \times w_{3,1}^3) : (y_1^2 \times f_0^2) + (Y_2^2 \times w_{2,1}^2) + (Y_1^2 \times w_{2,1}^1 + Y_3^3 \times w_{3,1}^3) = (3 \times 4) + 0 + (1 \times 2 + 0) : 0 + 0 + (3 \times 2 + 0) = 14 : 6$.

Similar to *FacDA* here also we need to impose some consistency constraints for each mixing nodes of TS_n in F_{TS}, which are detailed in **Appendix C3**. The set of linear and non-linear equations for determining the dilution graph G_D shown in Fig. 9(b) corresponding to the F_{TS} shown in Fig. 10(d) is illustrated in **Appendix C4**. The pseudo-code for this complete procedure *TVODA* is written as **Algorithm 3**. Here, we first generate the clauses corresponding to the equations and constraints as discussed above to form an SMT instance S (line no. 3). Moreover, in order to optimize the utilization of both *sample* and *buffer*, we use the Minimize() function in Z3 tool and update S by adding the corresponding clauses (line no. 3). Finally, we call the Optimize_SAT() function with S as an argument to obtain the satisfiable assignment of S, which determines the dilution graph G_D.

Algorithm 3: *TVODA*$(x : y, V_t, M)$

Input: Target ratio *sample* : *buffer* $= x : y$, where $x + y = N$, target volume V_t, and mixing volume constraint M
Output: Dilution graph G_D generating V_t unit volume of desired C_t

1 **begin**
2 Construct F_{TS} and obtain $\widehat{M}_\ell^m$, $\forall TS_m \in F_{TS}$; /* Discussed in Sec. IV-B1. */
3 S = (SMT instance for F_{TS}) $\wedge$ (arg min($\sum_{\forall TS_m \in F_{TS}} \sum_{i=0}^{d_m-1} (x_i^m + y_i^m)$));
4 Optimize_SAT(S);
5 Obtain dilution graph G_D from the satisfiable assignment of S;
6 **return** Dilution graph G_D;

V. Discussions on *FacDA* and *TVODA*

A. Priority of the Objective Parameters in FacDA and TVODA

Sample preparation is a multi-objective problem, where the objective is to minimize n_m, n_s and n_w simultaneously. The relationship among n_m, n_s and n_w largely depends on the structure of a dilution graph (skewed or non-skewed) and the ordering of the mixers used at different levels, so it is very hard to minimize all the variables simultaneously. Hence, most of the methods in the literature assigns a priority among n_m, n_s and n_w and then minimize them accordingly.

In *FacDA* we choose the structure of a dilution graph to be a skewed one and the general intuition is that with lesser n_m the whole problem becomes simpler because of the reduction in the number of variables. So initially we choose the lowest possible n_m, which can generate the target ratio maintaining the error tolerance ϵ (Sec. III-C). Then we focus on the minimization of n_s and n_w. In order to maintain the flow conservation in a dilution graph, $\sum w^n_{p,j} + n_w$ must be equals to $(n_s + n_b)$, i.e., $\sum w^n_{p,j} = n_s + n_b - n_w$. Here, $\sum w^n_{p,j}$ is inversely proportional to both n_s and n_w. Also, n_s and n_b are inversely proportional to each other, so it is very difficult to minimize both n_s and n_w simultaneously. Hence, we decide our primary objective as the minimization of n_s only. We maximize the scope of $\sum w^n_{p,j}$, minimize n_s and formulate the equations in such a way that the SAT solver is able to determine an overall efficient dilution graph.

In case of *TVODA* multiple skeleton trees are considered so there is also a scope for minimizing n_m. Along with the constraints of *FacDA* we also append the constraints for minimizing n_m and determine efficient dilution graphs for given target volumes using *TVODA*.

B. Scopes for FacDA and TVODA

The scope of any dilution algorithm presented in the literature primarily depend on its exploration of different mixing models. Both *FacDA* and *TVODA* can explore Mixer-M, which includes maximum number of mixing models. Also, in order to minimize n_s, *FacDA* and *TVODA* maximize the utilization of the sharing edges with the power of SMT solver. So, the dilution approaches for any other platforms (DMFB or CFMB) e.g., *twoWayMix*, *FloSPA-D* can never perform better than *FacDA*. This motivates us to consider the two most efficient dilution algorithms *WSPM* and *MRCM* for comparing the performances of *FacDA* and *TVODA*. In Table I, we present the scopes of all the dilution algorithms for all the three platforms, whose primary objective are either reagent minimization or mixing step minimization. From Table I we realize that *FacDA* is the first approach to consider Mixer-M and the utilization of sharing edges simultaneously. Moreover, *TVODA* minimize both n_m and n_s and also considers the target volume as another objective, which is beneficial for many real-life bio-protocols.

VI. Simulation Results

We implement all the three dilution algorithms namely *WSPM* [27], *MRCM* [28], and the proposed *FacDA* in Python.

TABLE I: Comparison of the scopes of different dilution algorithms designed for different microfluidic platforms.

Dilution Algo.	DMFB	CMFB	MEDA	Mixing Models	Minimize		Target Vol.	Reuse of Intermediate Fluids
					n_m	n_s		
twoWayMix	✓	×	×	1:1	–	–	×	×
REMIA	✓	×	×	1:1	–	✓	×	✓
VOSPA	✓	✓	×	RMixer-M	–	✓	×	✓
FloSPA-D	✓	✓	×	RMixer-M	–	✓	×	✓
WSPM	✓	partial	partial	$m:n$ $\in$ Mixer-M	–	✓	×	✓
MRCM	✓	✓	✓	Mixer-M	–	✓	×	×
FacDA	✓	✓	✓	Mixer-M	–	✓	×	✓
TVODA	✓	✓	✓	Mixer-M	✓	✓	✓	✓

The clauses in the SMT solver Z3 [29] for *FacDA* and *TVODA* are written using Python library Z3Py that can handle linear constraints with Boolean connectives. All simulations are performed in a computer with a 3.70 GHz Intel Xeon processor and 32 GB RAM running 64-bit Windows 10 OS.

A. Simulation Results for FacDA

MRCM is the most recent algorithm for sample preparation using MEDA biochips and primarily its objective is to determine the mixing tree with the minimum requirement of most costly reagent. However, *FacDA* deals with an automated dilution of fluids using MEDA biochips, where only two reagents are considered namely *sample* and *buffer*. For effective comparison, we consider only two reagents (*sample* and *buffer*) for *MRCM*, where the cost of *sample* is assumed to be greater than that of *buffer*. For each of these three variants of *MRCM*, we compare *FacDA* and generate the histogram plots of their performance parameters. In simulations, we randomly consider a set of 500 co-prime target ratios, where the ratio-sum N varies between 16 and 150 (i.e., $1:15, \cdots, 149:1$). For different mixing volume constraint $M \in \{4, 5, 6, 7\}$, and error-tolerance $\epsilon = 0.001$ the performance of *FacDA* is compared with *WSPM* and *MRCM* in terms of the number of mixing steps n_m, number of sample units n_s, number of waste units n_w and CPU time n_t (in sec.) required for execution. Fig. 11(a), (b), (c), and (d) presents the histogram plots of the average number of mixing steps ($\overline{n_m}$), average number of sample units ($\overline{n_s}$), and average number of waste units ($\overline{n_w}$), and average CPU time ($\overline{n_t}$), respectively, required for *WSPM*, *MRCM*, and *FacDA*. From the plots in Fig. 11(a) and Fig. 11(b) we can conclude that *FacDA* completely outperforms both *WSPM* and *MRCM*. In Fig. 11(c), for $M = 6, 7$, *FacDA* requires more n_w in compare to *MRCM*, but for all other cases *FacDA* manages to reduce n_w. As n_w is not strictly present in our optimization criteria, so although the n_w generation in *FacDA* is comparable with *WSPM* or *MRCM*, it is a bit unpredictable. Considering all the performance parameters, from these histogram plots we conclude that *FacDA* can generate efficient dilutions graphs. Moreover, Fig. 11(d) shows the distributions of $\overline{n_t}$ for the three methods, from which we can conclude the efficiency of *FacDA* over *WSPM* and *MRCM* in execution time also.

B. Simulation Results for TVODA

We compare the variations of n_m, n_s and n_w for the proposed method *TVODA* with those for *WSPM* and *MRCM* over different values of N, V_t and M. In simulations, we consider ratio-sum N as $20, 40, 60$ and 80, where $8, 16, 16$ and 32 are the number of unique co-prime target ratios, respectively. For each value of N and with a fixed $M = 6$, we consider V_t as $5, 10, 15$ and 20. Distributions of the average number of mixing steps $\overline{n_m}$, the average number of sample units $\overline{n_s}$, and the average number of waste units $\overline{n_w}$ for all the algorithms are shown in Figs. 12(a)-(d), Figs. 12(e)-(h) and Figs. 12(i)-(l), respectively. From Fig. 12, we conclude that $\overline{n_m}$, $\overline{n_s}$ and $\overline{n_w}$ increase proportionally with the increase in V_t for all three algorithms, however the lowest rate of this increment is seen

This article has been accepted for publication in a future issue of this journal, but has not been fully edited. Content may change prior to final publication. Citation information: DOI 10.1109/TCAD.2021.3063342, IEEE Transactions on Computer-Aided Design of Integrated Circuits and Systems

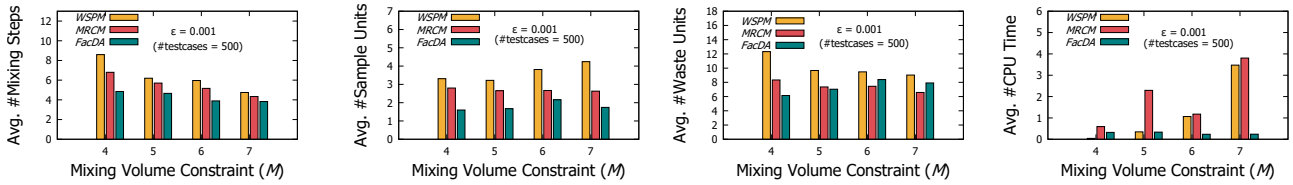

(a) (b) (c) (d)

Fig. 11: Comparison among *WSPM* [27], *MRCM* [28] and *FacDA* in the distributions of (a) $\overline{n_m}$, (b) $\overline{n_s}$, (c) $\overline{n_w}$, and (c) $\overline{n_t}$, for 500 random testcases of ratio-sum N ranging between $16-150$, with $M \in \{4,5,6,7\}$ and $\epsilon = 0.001$.

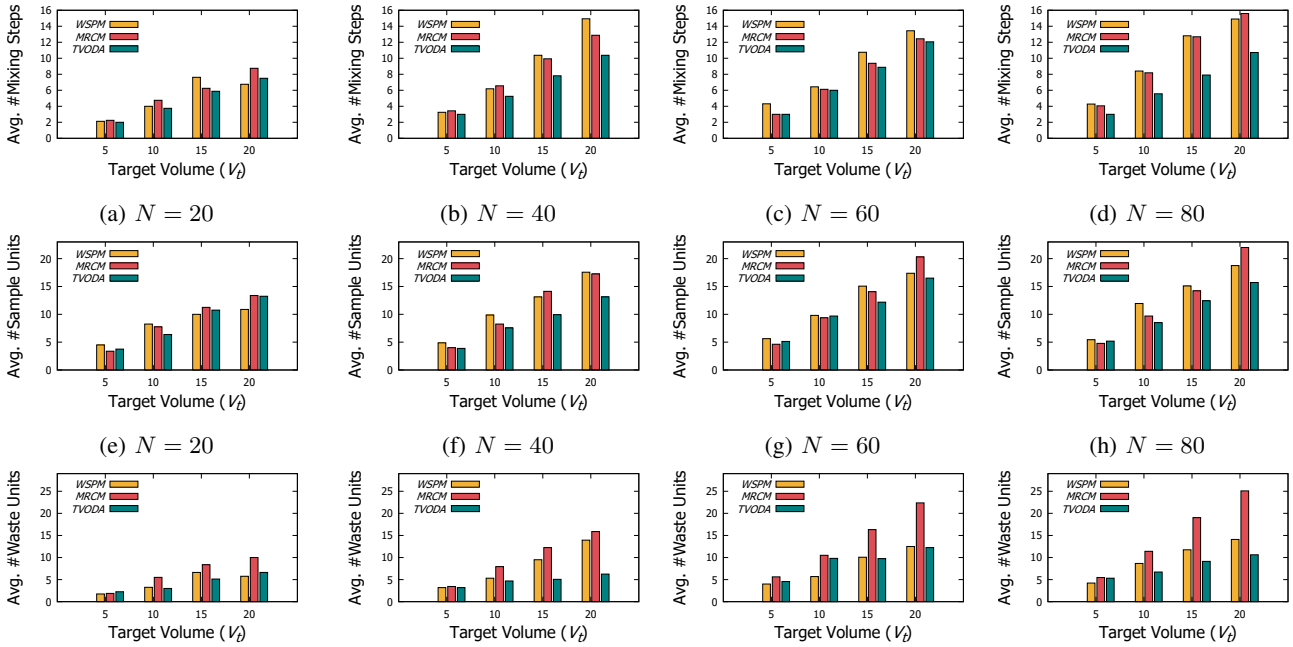

(a) $N = 20$ (b) $N = 40$ (c) $N = 60$ (d) $N = 80$

(e) $N = 20$ (f) $N = 40$ (g) $N = 60$ (h) $N = 80$

(i) $N = 20$ (j) $N = 40$ (k) $N = 60$ (l) $N = 80$

Fig. 12: Comparison among *WSPM* [27], *MRCM* [28] and *TVODA* in the distributions of (a)-(d) $\overline{n_m}$, (e)-(h) $\overline{n_s}$ and (i)-(l) $\overline{n_w}$, when $M = 6$ for ratio-sum $N \in \{20, 40, 60, 80\}$ and for target volume $V_t \in \{5, 10, 15, 20\}$.

for *TVODA*. In few instances, when V_t is 5 or 10, *TVODA* does not show better results compared to *WSPM* and *MRCM*, whereas *TVODA* starts outperforming others with increasing V_t. This is because the number of variables corresponding to the inter-skeleton sharing edges in F_{TS} is proportional to V_t. As the number of these variables increases, pruning of the mixing node(s) increases and subsequently it reduces n_m, n_s and n_w. Furthermore, with the increase in N, *TVODA* outperforms *WSPM* and *MRCM*, which implies that it is an efficient dilution algorithm for a given target volume. In other simulations, the performance of *TVODA* is examined by varying M with a fixed $V_t = 18$. For each case of N varying between 30 and 90, and M varying from the set $\{5, 7, 9\}$, we consider 100 random co-prime ratios. Table II provides the values of $\overline{n_m}$, $\overline{n_s}$ and $\overline{n_w}$ for all three algorithms. We observe that $\overline{n_m}$ decreases with increasing M for all three algorithms due to the availability of more mixing models, whereas *TVODA* outperforms with increasing M.

Table III depicts the advantages of *TVODA* over *WSPM* and *MRCM* in regard to n_m, n_s and n_w for four real-life bio-

TABLE II: Comparison among *WSPM* [27], *MRCM* [28] and *TVODA* when $V_t = 18$ with $M \in \{5, 7, 9\}$.

M	*WSPM*			*MRCM*			*TVODA*		
	$\overline{n_m}$	$\overline{n_s}$	$\overline{n_w}$	$\overline{n_m}$	$\overline{n_s}$	$\overline{n_w}$	$\overline{n_m}$	$\overline{n_s}$	$\overline{n_w}$
5	13.84	16.69	12.93	18.50	20.41	21	16.66	16.32	14.23
7	11.47	16.39	10.59	9.68	15.60	13.8	8.27	12.94	7.77
9	9.36	16.65	8.61	5.18	12.87	8.85	4.56	11.76	4.74

TABLE III: Comparison among *WSPM* [27], *MRCM* [28] and *TVODA* for 4 real-life bio-protocols†.

Bio-protocol Ratios	M	V_t	***WSPM***			***MRCM***			***TVODA***		
			n_m	n_s	n_w	n_m	n_s	n_w	n_m	n_s	n_w
Protein Assay [15] 1 : 127	4	8	8	2 (31.2 nL)	14	8	2 (31.2 nL)	14	7	1 (15.6 nL)	12
Glucose Assay [30] 1 : 319	6	10	8	2 (31.2 nL)	20	10	2 (31.2 nL)	16	6	1 (15.6 nL)	10
RNA extraction from worms [31] 486 : 26	6	6	17	18 (280.8 nL)	15	10	12 (187.2 nL)	14	4	8 (124.8 nL)	3
In vitro culture of human PBMCs [31] 51 : 461	6	6	3	3 (46.8 nL)	6	14	4 (62.4 nL)	20	4	1 (15.6 nL)	7

†one droplet has a volume of 4 * 3.9 nL, where the droplet size is 4X with 3.9 nL capacity of each microelectrode [14].

protocols. In all these cases n_s is the smallest in *TVODA* and thus, it reduces sample cost significantly compared to previous algorithms for MEDA chips. An executable file of our proposed approaches can be accessed form: https://dkundu-1.github.io/FacDA.github.io/.

VII. Conclusions

In this paper we have brought into light some inherent combinatorial properties that govern the generic sample preparation supported by microfluidic biochips and their relationships with various mixing models. We show that prime factorization and partitioning of integers play a major role in optimizing the dilution process given the physical constraints of the underlying platform. Based on these properties, we study the interdependence of mixer architectures and propose two factorization-based algorithms namely *FacDA* and *TVODA* that are capable of generating a target ratio of two fluids using MEDA biochips.

Both of them are capable of utilizing different mixing models supported by MEDA. *FacDA* can determine a sequence of mixing models and generate a dilution graph with minimum sample usage. *TVODA* can determine a dilution graph for a target ratio with any desired volume. The optimum sequence of mixing models to achieve the best dilution graph is left as an open problem.

Acknowledgement

The authors would like to thank Prof. Philip Brisk and the anonymous reviewers for their critical comments and valuable suggestions.

References

[1] S. Saha, D. Kundu, S. Roy, S. Bhattacharjee, K. Chakrabarty, P. P. Chakrabarti, and B. B. Bhattacharya, "Factorization Based Dilution of Biochemical Fluids with Micro-Electrode-Dot-Array Biochips," in *Proc. of the ASP-DAC*, 2019, pp. 462–467.

[2] J. Melin and S. R. Quake, "Microfluidic Large-Scale Integration: The Evolution of Design Rules for Biological Automation," *Annual Review of Biophysics and Biomolecular Structure*, vol. 36, no. 1, pp. 213–231, 2007.

[3] I. E. Araci and S. R. Quake, "Microfluidic Very Large Scale Integration (mVLSI) with Integrated Micromechanical Valves," *Lab Chip*, vol. 12, no. 16, pp. 2803–2806, 2012.

[4] J. Fowler, H. Moon, and C.-J. Kim, "Enhancement of Mixing by Droplet-Based Microfluidics," in *Proc. of the IEEE MEMS*, 2002, pp. 97–100.

[5] V. Gubala, L. F. Harris, A. J. Ricco, M. X. Tan, and D. E. Williams, "Point of Care Diagnostics: Status and Future," *Analytical Chemistry*, vol. 84, no. 2, pp. 487–515, 2012.

[6] A. G. Uren, H. Mikkers, J. Kool, L. van der Weyden, A. H. Lund, C. H. Wilson, R. Rance, J. Jonkers, M. van Lohuizen, A. Berns, and D. J. Adams, "A High-Throughput Splinkerette-PCR Method for the Isolation and Sequencing of Retroviral Insertion Sites," *Nature Protocols*, vol. 4, no. 5, pp. 789–798, 2009.

[7] S. Srigunapalan, I. A. Eydelnant, C. A. Simmons, and A. R. Wheeler, "A Digital Microfluidic Platform for Primary Cell Culture and Analysis," *Lab Chip*, vol. 12, no. 2, pp. 369–375, 2012.

[8] S. Einav, D. Gerber, P. D. Bryson, E. H. Sklan, M. Elazar, S. J. Maerkl, and S. R. Quake, "Discovery of a Hepatitis C Target and its Pharmacological Inhibitors by Microfluidic Affinity Analysis," *Nature Biotechnology*, vol. 26, no. 9, pp. 1019–1027, 2008.

[9] H. C. Fan, Y. J. Blumenfeld, U. Chitkara, L. Hudgins, and S. R. Quake, "Noninvasive Diagnosis of Fetal Aneuploidy by Shotgun Sequencing DNA from Maternal Blood," *Proc. National Academy of Sciences*, vol. 105, no. 42, pp. 16 266–16 271, 2008.

[10] C. Fang, Y. Wang, N. T. Vu, W. Lin, Y. Hsieh, L. Rubbi, M. E. Phelps, M. Mueschen, Y. Kim, A. F. Chatziioannou, H. Tseng, and T. G. Graeber, "Integrated Microfluidic and Imaging Platform for a Kinase Activity Radioassay to Analyze Minute Patient Cancer Samples," *Cancer Research*, vol. 70, no. 21, pp. 8299–8308, 2010.

[11] R. B. Fair, V. Srinivasan, H. Ren, P. Paik, V. K. Pamula, and M. G. Pollack, "Electrowetting-Based On-Chip Sample Processing for Integrated Microfluidics," in *Proc. of the IEEE IEDM*, 2003, pp. 32.5.1–32.5.4.

[12] P. Y. Paik, V. K. Pamula, M. G. Pollack, and R. B. Fair, "Electrowetting-Based Droplet Mixers for Microfluidic Systems," *Lab Chip*, vol. 3, no. 1, pp. 28–33, 2003.

[13] G. Wang, D. Teng, and S.-K. Fan, "Digital Microfluidic Operations on Micro-Electrode Dot Array Architecture," *IET Nanobiotechnology*, vol. 5, no. 4, pp. 152–160, 2011.

[14] B. Hadwen, G. R. Broder, D. Morganti, A. Jacobs, C. Brown, J. R. Hector, Y. Kubota, and H. Morgan, "Programmable Large Area Digital Microfluidic Array with Integrated Droplet Sensing for Bioassays," *Lab Chip*, vol. 12, no. 18, pp. 3305–3313, 2012.

[15] K. Chakrabarty and F. Su, *Digital Microfluidic Biochips: Synthesis, Testing and Reconfiguration Techniques*. CRC Press, 2007.

[16] S. Bhattacharjee, B. B. Bhattacharya, and K. Chakrabarty, *Algorithms for Sample Preparation with Microfluidic Lab-on-Chip*. River Publishers, 2019.

[17] S. Roy, B. B. Bhattacharya, and K. Chakrabarty, "Optimization of Dilution and Mixing of Biochemical Samples using Digital Microfluidic Biochips," *IEEE TCAD*, vol. 29, no. 11, pp. 1696–1708, 2010.

[18] J. D. Huang and C. H. Liu and H. S. Lin, "Reactant and Waste Minimization in Multitarget Sample Preparation on Digital Microfluidic Biochips," *IEEE TCAD*, vol. 32, no. 10, pp. 1484–1494, 2013.

[19] C.-H. Liu, H.-H. Chang, T.-C. Liang, and J.-D. Huang, "Sample Preparation for Many-Reactant Bioassay on DMFBs using Common Dilution Operation Sharing," in *Proc. of the ICCAD*, 2013, pp. 615–621.

[20] T. A. Dinh, S. Yamashita, and T.-Y. Ho, "A Network-flow-based Optimal Sample Preparation Algorithm for Digital Microfluidic Biochips," in *Proc. of the ASP-DAC*, 2014, pp. 225–230.

[21] C. H. Liu, T. W. Chiang, and J. D. Huang, "Reactant Minimization in Sample Preparation on Digital Microfluidic Biochips," *IEEE TCAD*, vol. 34, no. 9, pp. 1429–1440, 2015.

[22] L. Shao, Y. Yang, H. Yao, T.-Y. Ho, and Y. Cai, "LUTOSAP: Lookup Table Based Online Sample Preparation in Microfluidic Biochips," in *Proc. of the GLSVLSI*, 2017, pp. 447–450.

[23] Shalu, S. Kumar, A. Singla, S. Roy, K. Chakrabarty, P. P. Chakrabarti, and B. B. Bhattacharya, "Demand-Driven Single- and Multitarget Mixture Preparation using Digital Microfluidic Biochips," *ACM TODAES*, vol. 23, no. 4, pp. 55:1–55:26, 2018.

[24] S. Bhattacharjee, S. Poddar, S. Roy, J. D. Huang, and B. B. Bhattacharya, "Dilution and Mixing Algorithms for Flow-Based Microfluidic Biochips," *IEEE TCAD*, vol. 36, no. 4, pp. 614–627, 2017.

[25] C.-M. Huang, C.-H. Liu, and J.-D. Huang, "Volume-Oriented Sample Preparation for Reactant Minimization on Flow-based Microfluidic Biochips with Multi-segment Mixers," in *Proc. of the DATE*, 2015, pp. 1114–1119.

[26] W. Thies, J. P. Urbanski, T. Thorsen, and S. Amarasinghe, "Abstraction Layers for Scalable Microfluidic Biocomputing," *Natural Computing*, vol. 7, no. 2, pp. 255–275, 2008.

[27] Z. Li, K. Y. T. Lai, K. Chakrabarty, T. Y. Ho, and C. Y. Lee, "Droplet Size-Aware and Error-Correcting Sample Preparation Using Micro-Electrode-Dot-Array Digital Microfluidic Biochips," *IEEE TBCAS*, vol. 11, no. 6, pp. 1380–1391, 2017.

[28] T. C. Liang, Y. S. Chan, T. Y. Ho, K. Chakrabarty, and C. Y. Lee, "Sample Preparation for Multiple-Reactant Bioassays on Micro-Electrode-Dot-Array Biochips," in *Proc. of the ASP-DAC*, 2019, pp. 468–473.

[29] L. de Moura and B. Nikolaj, "Z3: An Efficient SMT Solver," in *Proc. of the TACAS*, 2008, pp. 337–340.

[30] Glucose Assay, ScienCell Research Laboratories, CA, USA., https://www.sciencellonline.com/PS/8418.pdf, [Accessed on December 2020].

[31] S. Poddar, S. Ghoshal, K. Chakrabarty, and B. B. Bhattacharya, "Error-Correcting Sample Preparation with Cyberphysical Digital Microfluidic Lab-on-Chip," *ACM TODAES*, vol. 22, no. 1, 2016.

Debraj Kundu received the B.Tech. degree in computer science and engineering from the Maulana Abul Kalam Azad University of Technology (formerly, known as the West Bengal University of Technology), in 2014 and, the M.Tech. degree in computer science and engineering from the University of Calcutta, Kolkata, India, in 2016. He is currently pursuing the Ph.D. degree from Indian Institute of Technology Roorkee, Roorkee, India.

His current research interests include algorithms for computer-aided design of advanced microfluidic biochips.

Sudip Roy (S'10–M'14) received the B.Sc. degree (Hons.) in physics and the B.Tech. degree in computer science and engineering from the University of Calcutta, India, in 2001 and 2004, respectively, and the M.S. (by research) and Ph.D. degrees in computer science and engineering from the Indian Institute of Technology (IIT) Kharagpur, India, in 2009 and 2014, respectively. He is currently an assistant professor in the department of computer science and engineering, IIT Roorkee, India since July 2014. He is also an associated faculty member of the centre of excellence in disaster mitigation and management (CoEDMM) in IIT Roorkee, India since April 2015. He has authored one book, one book chapter, two granted U.S. patents, one filed U.S. patent, and two filed Indian patents.

His current research interests include computer-aided-design for digital systems, optimization techniques, information and communication technologies (ICT) for disaster risk reduction (DRR). He is a member of IEEE and ACM.

Sukanta Bhattacharjee received the B.Sc. (Hons.) degree in computer science and the B.Tech. degree in computer science and engineering from the University of Calcutta, India, in 2006 and 2009 respectively. He received the M.Tech. and Ph.D. degree in computer science from the Indian Statistical Institute, Kolkata, India, in 2012 and 2017 respectively. He is working as an assistant professor in the Department of Computer Science and Engineering at Indian Institute of Technology, Guwahati, India. Before that he worked for two years as a postdoctoral fellow at the Center for Cyber Security, New York University Abu Dhabi (NYUAD), UAE. He also worked as a visiting scientist at the Advanced Computing and Microelectronics Unit, Indian Statistical Institute, Kolkata, India.

His research interests include Design Automation Algorithms, Microfluidics, and Security.

Sohini Saha is currently a software developer at PwC India, creating and delivering web applications in an agile environment. She has received the B.Tech degree from the Indian Institute of Engineering Science and Technology (IIEST), Shibpur in 2019.

Her current research interests include building secure and resilient hardware while using machine learning techniques, microfluidic biochips and silicon photonics.

Krishnendu Chakrabarty received the B. Tech. degree from the Indian Institute of Technology, Kharagpur, in 1990, and the M.S.E. and Ph.D. degrees from the University of Michigan, Ann Arbor, in 1992 and 1995, respectively. He is now the John Cocke Distinguished Professor and Department Chair of Electrical and Computer Engineering (ECE), and Professor of Computer Science, at Duke University.

Prof. Chakrabarty is a recipient of the National Science Foundation CAREER award, the Office of Naval Research Young Investigator award, the Humboldt Research Award from the Alexander von Humboldt Foundation, Germany, the IEEE Transactions on CAD Donald O. Pederson Best Paper Award (2015), the ACM Transactions on Design Automation of Electronic Systems Best Paper Award (2017), multiple IBM Faculty Awards and HP Labs Open Innovation Research Awards, and over a dozen best paper awards at major conferences. He is also a recipient of the IEEE Computer Society Technical Achievement Award (2015), the IEEE Circuits and Systems Society Charles A. Desoer Technical Achievement Award (2017), the Semiconductor Research Corporation Technical Excellence Award (2018), and the IEEE Test Technology Technical Council Bob Madge Innovation Award (2018). He is a Research Ambassador of the University of Bremen (Germany) and he was a Hans Fischer Senior Fellow at the Institute for Advanced Study, Technical University of Munich, Germany during 2016-2019. He is a 2018 recipient of the Japan Society for the Promotion of Science (JSPS) Invitational Fellowship in the "Short Term S: Nobel Prize Level" category.

Prof. Chakrabarty's current research projects include: design-for-testability of integrated circuits and systems (especially 3D integration and system-on-chip); microfluidic biochips; hardware security; machine learning for fault diagnosis, failure prediction, healthcare, and biochemical analysis; neuromorphic computing systems. He is a Fellow of ACM, a Fellow of IEEE, a Fellow of AAAS, and a Golden Core Member of the IEEE Computer Society. He was a Distinguished Visitor of the IEEE Computer Society (2005-2007, 2010-2012), a Distinguished Lecturer of the IEEE Circuits and Systems Society (2006-2007, 2012-2013), and an ACM Distinguished Speaker (2008-2016). Prof. Chakrabarty served as the Editor-in-Chief of IEEE Design and amp; Test of Computers during 2010-2012, ACM Journal on Emerging Technologies in Computing Systems during 2010-2015, and IEEE Transactions on VLSI Systems during 2015-2018.

Partha Pratim Chakrabarti received the B.Tech. and Ph.D. degrees in Computer Science and Engineering from the Indian Institute of Technology Kharagpur (IIT), Kharagpur, India, in 1985 and 1988, respectively. Since 1988, he has been a Faculty Member with IIT Kharagpur, where he is currently a Professor in the Department of Computer Science and Engineering and former Director of the Institute. He has published more than 250 research papers and has successfully completed several major research projects. His areas of interest include AI, CAD for VLSI and Embedded Systems. Prof. Chakrabarti was the recipient of several honors, including the President of India Gold Medal, the Swarnajayanti Fellowship and the Shanti Swarup Bhatnagar Prize from the Government of India for his contributions. He is a Fellow of Indian National Science Academy, Indian National Academy of Engineering, Indian Academy of Science and a senior member of the IEEE.

Bhargab B. Bhattacharya (F '07) is currently serving as Distinguished Visiting Professor of Computer Science and Engineering at the Indian Institute of Technology Kharagpur. Prior to that, he had been on the faculty of the Indian Statistical Institute, Kolkata, for over 35 years. His research interest includes digital logic testing, and electronic design automation for integrated circuits and microfluidic biochips. He has published more that 400 technical papers and he holds ten US Patents. He is a Fellow of the Indian National Academy of Engineering and a Fellow of the National Academy of Sciences (India).